Journal of Structural Biology 165 (2009) 133–139

Contents lists available at ScienceDirect

Journal of Structural Biology

journal homepage: www.elsevier.com/locate/yjsbi

Crystal structures of the Apo and Holo form of rat catechol-*O*-methyltransferase

Eiichi Tsuji [a,b,*], Kosuke Okazaki [a], Masayuki Isaji [a], Kei Takeda [b]

[a] Molecular Design Research, R&D Kissei Pharmaceutical Co., Ltd. 4365-1 Kashiwabara, Hotaka, Azumino-city, Nagano 399-8304, Japan
[b] Department of Synthetic Organic Chemistry, Graduate School of Biomedical Sciences. 1-2-3 Kasumi, Minami-Ku, Hiroshima 734-8553, Japan

ARTICLE INFO

Article history:
Received 11 April 2008
Received in revised form 3 October 2008
Accepted 25 November 2008
Available online 10 December 2008

Keywords:
Apo form
Holo form
Catechol-*O*-methyltransferase
X-ray crystal structure

ABSTRACT

Catechol-*O*-methyltransferase (COMT, EC 2.1.1.6) is a monomeric enzyme that catalyzes the transfer of a methyl group from *S*-adenosyl-L-methionine (AdoMet) to the phenolic oxygen of substituted catechols. Although the inhibitor recognition pattern and AdoMet site have already been studied crystallographically, structural information on the catalytic cycle of COMT has not yet been obtained. In this study, comparison of the co-factor and inhibitor-bound structures revealed that the Apo form of COMT shows a conformational change and there was no cleft corresponding to the AdoMet-binding site; the overall structure was partially open form and the substrate recognition site was not clearly defined. The Holo form of COMT was similar to the quaternary structure except for the β6–β7 and α2–α3 ligand recognition loops. These conformational changes provide a deeper insight into the structural events occurring in reactions catalyzed by AdoMet.

1. Introduction

Catechol-*O*-methyltransferase (COMT, EC 2.1.1.6) plays an important role in the catabolic inactivation of biologically active or toxic catechols. The physiological substrates of COMT are catecholamine neurotransmitters, such as dopamine, noradrenaline, and adrenaline. In mammals, COMT is distributed in various organs (Karhunen et al., 1994), and highest levels of activity are found in the liver and kidney. Considerable clinical interest has been shown in COMT because of the possibility of using COMT inhibitors as adjuncts in L-DOPA therapy for Parkinson's diseases (PD). L-DOPA is a precursor of dopamines and is metabolized in extracerebral tissues and the central nervous system. The symptoms of PD are a consequence of reduced levels of dopamine in the brain due to degeneration of dopaminergic neurons. There is an urgent need to ensure a more sustained regimen of L-DOPA supply to PD patients to counteract disease symptoms. COMT is one of the main enzymes of L-DOPA metabolism (Guldberg and Marsden, 1975), and new potent and selective COMT inhibitors have become available (Männistö and Kaakkola, 1989; Kaakkola et al., 1990). Two of these, tolcapone and entacapone are currently being used clinically to treat PD. These drugs exert profound influences on L-DOPA kinetics by increasing its bioavailability and half-life, thus allowing more stable L-DOPA plasma levels to be obtained orally and, as a result, more sustained dopaminergic brain stimulation (Männistö and Kaakkola, 1999). COMT catalyzes the transfer of the methyl group from the coenzyme AdoMet to one of the hydroxyls of catechol or substituted catechols in the presence of an Mg^{2+} ion. The catalytic mechanism of COMT has been extensively discussed on the basis of structural, biochemical, and theoretical studies (Vidgren et al., 1994; Lotta et al., 1995; Edmond and Thomas, 2000). The enzymatic reaction likely proceeds by an order sequential kinetics mechanism with AdoMet-binding first, followed by an Mg^{2+} ion, and then by the catechol substrate. AdoHcy (*S*-adenosyl-L-homocysteine) is the last ligand released in the catalytic cycle (Lotta et al., 1995). The chemical step of the reaction was revealed to be an S_N2-like process (Woodard et al., 1980), and results of structural studies indicated that AdoMet bound to the deep cleft of COMT and made many interactions with amino acids. As a result of various hydrogen bonds and van der Waals contacts, AdoMet has an affinity for COMT with a dissociation constant of 23 μM (Lotta et al., 1995). The turnover rate of COMT is very slow, and the binding affinity of AdoHcy is very similar to that of AdoMet. There are almost no atoms of AdoMet in contact with the solvent on the surface of COMT. Thus, it is reasonable to speculate that a large conformational change may be involved in the AdoMet-binding and AdoHcy releasing process. Recently published COMT structures, which were complexed with various inhibitors, have provided considerable insight into the recognition of substrates (Palma et al., 2006; Bonifacio et al., 2002; Lerner et al., 2001). However, structural information showing how COMT provides both a co-factor and a substrate-binding site has not been obtained. In this study, we expressed rat S-COMT (soluble COMT) at high levels in an *Escherichia coli* system and purified it to homogeneity. The Apo and Holo forms of S-COMT were then crystallized, and their

* Corresponding author. Address: Molecular Design Research, R&D Kissei Pharmaceutical Co., Ltd. 4365-1 Kashiwabara, Hotaka, Azumino-city, Nagano 399-8304, Japan. Fax: +81 0263 82 8827.
E-mail address: eiichi_tsuji@pharm.kissei.co.jp (E. Tsuji).

1047-8477/$ - see front matter © 2008 Elsevier Inc. All rights reserved.
doi:10.1016/j.jsb.2008.11.012

three-dimensional structures were determined. Following comparison with other published structures, we then discuss how S-COMT is able to change its structural links in recognition of various substrates.

2. Materials and methods

2.1. Protein expression and purification

Protein expression and purification methods were referenced by the previously published method (Tilgman and Ulmanen, 1996; Lundstrom et al., 1992). A truncate form of rat S-COMT was designed as amino acids 1–221 having an N-terminal GST-tag fusion protein. Template DNA (full-length rat COMT (NCBI: M60754)) was amplified with the primers. Rat S-COMT N-GST forward (5′-tctggatcca tgggtgacac aaaggagcag-3′) rat S-COMT N-GST reverse (5′-agagaattct caagacttgt cagggctac-3′). The expressed recombinant protein after thrombin digestion had the artificially introduced start sequence Gly, Ser, and the natural C-terminus of the sequence of S-COMT. PCR reactions were carried out for 40 cycles in an Eppendorf mastercycler gradient under the following conditions: denaturation at 94 °C for 2.25 min, annealing at 59 °C for 30 s, and extension at 68 °C for 60 s. Final extension was achieved at 68 °C for 55 min and at 4 °C for 10 min. Rat S-COMT N-GST coding DNA was then digested with BamHI and EcoRI. The digested PCR product was ligated into the pGEX-2T vector and denoted as rat S-COMT N-GST-pGEX-2T. *E. coli* JM109 was transformed with rat S-COMT N-GST-pGEX-2T, and the transformant was grown in an LB plate supplemented with 100 μg/ml ampicillin for 15 h at 37 °C. A single colony was selected and purified by using a Qiagen plasmid mini kit (Qiagen). The purified plasmid was authenticated by DNA sequencing and denoted as rat S-COMT N-GST-JM109. *E. coli* BL21 CODON PLUS (DE3) RP was transformed with the rat S-COMT N-GST-JM109, and the resulting transformant was grown on an LB plate supplemented with 100 μg/ml ampicillin for 15 h at 37 °C. A single colony was again selected and shaken in 10 ml of LB-ampicillin medium for 4 h at 37 °C. Afterwards, 10 ml of pre-cultured cells were grown at 37 °C in 500 ml of LB medium containing 100 μg/ml ampicillin until OD at 600 nm reached 0.24. Protein expression was induced by 0.1 mM isopropyl-β-D-thiogalactopyranoside for 6 h at 20 °C. Cells were harvested by centrifugation and lysed in a BugBuster (Novagen) at ambient temperature for 15 min. The soluble bacterial extracts was isolated by centrifugation and then added to a 50% suspension of GST 4B Sepharose resin (GE Healthcare Biosciences) equilibrated in D-PBS (DULBECCO'S Phosphate Buffered Saline). The resin mixture was separated and washed with 150 mM NaCl, 10% glycerol, 2.5 mM $CaCl_2$, and 0.5% β-octyl-D-glucopyranoside in 50 mM Tris buffer (pH 8.0). To remove the GST-tag, the recombinant S-COMT was digested with thrombin (GE Healthcare Biosciences) in the resin-wash buffer at 4 °C for 15 h. The digested mixture was loaded into an empty column and the flow through was pooled. The flow-through fraction was applied to a GSTrap FF column (GE Healthcare Biosciences) to remove the uncut form of the fusion protein, and the molecular weight of the partially purified recombinant protein was checked by ESI Q-pole mass spectroscopy (Waters ZQ4000). The molecular weight of recombinant S-COMT was 24889.43, which coincided with the theoretical value of 24891.63. The eluted fraction from the GSTrap FF was further subjected to Super Q-5PW (TOSOH) equilibrated in 10 mM NaCl, 10% glycerol, 4.0 mM DTT, 0.5% β-octyl-D-glucopyranoside, and 1.0 mM EDTA in 20 mM Tris buffer (pH 7.0). Recombinant S-COMT was eluted with a linear gradient of NaCl (10–700 mM). The obtained fraction was concentrated with an YM-10 (Millipore) and subjected to gel filtration on a Superdex 16/60 HR75 prep grade (GE Healthcare Biosciences) with 50 mM MES buffer (pH 6.5) containing 1.0 mM DTT, 1.0 mM EDTA, and 10% glycerol. An enzyme activity assay of recombinant S-COMT was performed as described previously (Zücher and Da Prada, 1982), and demonstrated that the enzymatic activity of recombinant S-COMT was the same as that of full-length rat S-COMT.

2.2. Crystallization of Apo and Holo forms

The purified recombinant S-COMT solution was concentrated using an Amicon concentrator with an YM-10 membrane to 4.8–5.0 mg/ml in the gel-filtration buffer. The Apo and Holo forms of the crystals were set up at ambient temperature using the hanging-drop method (McPherson, 1990). Prior to crystallization of the Holo form, the co-factor AdoMet and $MgCl_2$ were added at three times the molar amount of the enzyme. Droplets containing protein and precipitant solution in equal amounts (2.0 μl) were equilibrated against 0.5 ml of reservoir solution. The Apo crystals suitable for diffraction study were grown from 0.2 M $(NH_4)_2SO_4$, 30% (w/v) PEG8000. The Holo form of crystals were grown from 0.2 M $(NH_4)_2SO_4$, 26% (w/v) PEG8000, 0.2% (v/v) sucrose.

2.3. Data collection and structure determination

Prior to data collection, the Apo and Holo crystals were separately transferred into a cryoprotectant solution containing 20% glycerol crystallization buffer. The crystals were then immediately flash-frozen and stored in liquid nitrogen until use. X-ray diffraction data were obtained at 100 K on a Pharmaceutical Consortium of Protein Research beam line (BL32B2) at SPring-8, Hyogo, Japan. The complete data sets were integrated and scaled using MOSFLM (Leslie, 1992) and SCALA (CCP4, 1994). The S-COMT structure reported by Vidgren et al. (PDB code: 1vid), without ligand, was used directly in molecular replacement trials employing AMoRe (Navaza, 1994). The primary phase was successfully assigned and further structural refinement was performed with CNX software (Accerlys, Japan). The structure was completed in altering cycles of manual model building with QUANTA (Accerlys, Japan). The crystallographic statistics are summarized in Table 1. N-terminus GSMG and C-terminus PSSPDKS residues were invisible due to their high thermal motion.

3. Results and discussion

3.1. Overall structure

S-COMT has a single-domain α/β-folded structure in which eight α-helices are arranged around the seven central β-sheets. The sheet contains five parallel β-strands and one antiparallel β-hairpin. The loop region between β1 and αA forms an AdoMet-binding consensus region that is conserved in methyltransferases (Vidgren et al., 1994). The overall arrangement of helices and strands in our study was almost the same in the Apo form of S-COMT and the inhibitor-bound structure (PDB code: 1vid), but the α1 and αB helices were shifted by 2.0 and 2.2 Å, respectively. The displacements of those two helices were larger than those of other helices. The most striking differences were found in the loop regions connecting β6–β7, α2–α3, β5–αE, and β4–αD. A comparison of the Apo form of S-COMT and inhibitor-bound structure is shown in Fig. 1A. The loop structure connecting α2–α3 contains Met40 and Val42, which directly interacted with AdoMet, and moved by a maximum 11.9 Å. The displacement of the β4–αD connecting loop, which formed an adenine ring-bound pocket, was 3.8 Å (Cα distance of His142 between the Apo form and inhibitor-bound structure (PDB code: 1vid)). In the Apo form, the side chain of His142 and Trp143 contained in β4–αD occupied the AdoMet-binding pocket. It has been noted that the Glu199 contained in β6–β7 participates directly in the methylation reaction in the

Table 1
Data collection and refinement statistics of Apo and Holo forms of S-COMT.

	Apo	Holo
(A) Data collection and processing		
Wavelength (A)	1.00	1.00
Space group	$P3_121$	$P2_12_12_1$
Unit cell parameters		
a, *b*, *c* (Å)	56.26, 56.26, 117.48	32.90, 61.09, 105.37
α, β, γ (deg.)	90, 90, 120	90, 90, 90
(B) Diffraction data		
Resolution range (Å)	39.22–2.20	39.0–2.60
Unique reflections	81 710	46 918
R (*I*) sym (%)	8.3	10.1
Completeness (%)	98.70	100.00
Redundancy	7.90	6.80
I/σ (*I*)	12.60	14.00
(C) Refinement		
Resolution range (Å)	2.20	2.60
Reflections used in refinement	11 356	6 225
Final *R* value (work/free)	0.20/0.26	0.19/0.28
Protein residues	211	205
Water molecules	183	42
Ligand	1	2
RMSD from ideal		
Bond lengths (Å)	0.02	0.02
Bond angles (deg.)	2.14	2.00
Ramachandran statistics		
Most favored regions (%)	94.1	91.1
Additionally allowed regions (%)	5.90	8.30
Mean B-factor (Å^2)		
Protein	15.8	32.3
Water molecules	22.1	28.0
Ligand	17.00	31.3/47.8

[a] $R\text{sym} = \Sigma_h\Sigma_i|I(h,i) - \langle I(h)\rangle|/\Sigma_h\Sigma_i I(h,i)$, where $I(h,i)$ is the intensity value of the *i*th measurement of *h* and $\langle I(h)\rangle$ is the corresponding mean value of $I(h)$ for all *i* measurements.
[b] $R\text{-work} = \sum||F_{obs}| - |F_{calc}||/|F_{obs}|$, where $|F_{obs}|$ and $|F_{calc}|$ are the observed and calculated structure factor amplitudes, respectively.
[c] *R*-free is the same as *R*-factor, but for a 5.0% subset of all reflections for Apo form and 10.0% for Holo form, respectively.

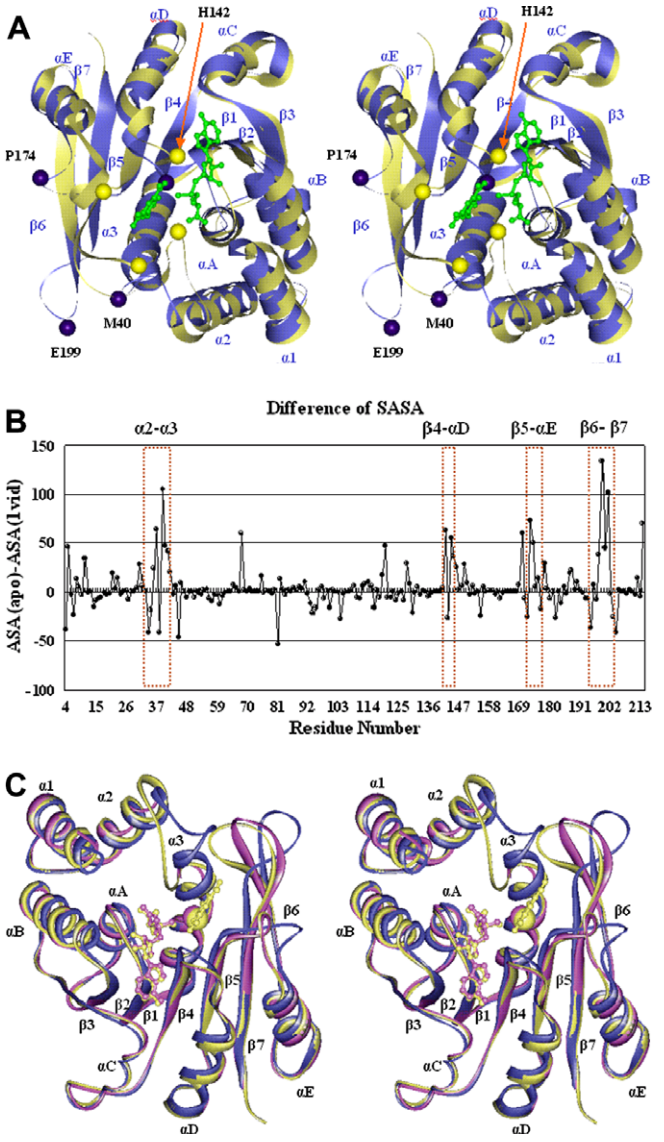

Fig. 1. (A) The Apo form of S-COMT is superimposed with the quaternary structure of S-COMT (PDB code: 1vid). Blue represents Apo form, pale yellow represents 1vid, and blue and pale yellow CPK represent the Cα atoms. The structural changes between the Apo and complex form are shown by red arrows. The ball and stick models represent AdoMet and 3,5-dinitrocatechol. For clarity, the sulfate ion derived from the crystallization buffer in the Apo structure and Mg^{2+} ion from the Holo structure are not shown. (B) Differences in the solvent-accessible surface areas between the Apo form and quaternary complex structure of S-COMT (PDB code: 1vid). Residue numbering coincides with the quaternary complex of S-COMT. Solvent-exposed residues are demarcated by dotted orange rectangles. Solvent-accessible surface area was calculated with AREAIMOL software (CCP4 Version. 6.0.1). (C) Apo and Holo forms of S-COMT are superimposed with quaternary structure (PDB code: 1vid). Blue represents Apo, cyan represents Holo, pale yellow represents 1vid. AdoMet and the Mg^{2+} ion are depicted as ball and stick representations. (A–C) were produced with WebLab Viewer Lite 5.0 (Accerlys, Japan).

known crystal structures of S-COMT. Here, the Cα of Glu199 moved by 13.7 Å. Lastly, the Pro174 contained in β5–αE defines the selectivity of the enzyme to different side chains of the substrate (Vidgren et al., 1994). The Cα of Pro174 moved by 8.6 Å. Insight from the known structures, which were complexed with various inhibitors, the β6–β7 and β5–αE connecting loops were participated in the forming of the ligand-binding site. However, in the Apo form, these loops were highly exposed to the solvent and a distinct ligand accommodation site had disappeared; the Apo form of S-COMT adopted a partially open form compared with previously published structures. The solvent-accessible surface areas (SASAs) of the α2–α3, β5–αE, β6–β7, and β4–αD loops were all larger than the other structural elements (Fig. 1B). In the Holo form, the α2-α3 loop structure was highly disordered and could not be determined their position. The β5–αE and β4–αD loops moved to almost the same position as that of quaternary structure. Interestingly, the β6–β7 loop, which contains Glu199, was found in the partially closed conformation (Fig. 1C). The key residues that participated in the recognition of AdoMet and the ligand were mainly located in the loop structure. AdoMet recognition residues on the loop were moved slightly upon structural changes between Apo and inhibitor-bound forms, with the exception of the α2–α3 loop. However, the ligand recognition residues moved significantly, suggesting that ligand-binding loops alter their structure for various sizes of ligands. Recently, an MD simulation structure of rat S-COMT (Bunker et al., 2008) showed that the position of each helix and sheet determined from the crystal structure of the Apo enzyme adopted almost the same position as that of the Holo and quaternary complex structures. However, the relative position of helixes and sheets determined from a 70 ns MD simulation structure was quite different from that of Apo structure; hydrogen bond-mediated helix–helix, helix–sheet, and sheet–sheet interactions might have been broken under the energy minimization steps and loosened the overall structure. Higher mobility was observed in the loop regions, particularly centered at residues Tyr200, Met40, and Gly175 during the simulation run. In the crystal structure, the α2–α3 and β5–αE loops, which contained Met40 and Gly175, respectively, represented a higher thermal factor than the

other parts. These observations were the almost identical in spite of the different methodologies.

3.2. AdoMet bound site

The active-site residues that have significant interactions with AdoMet have been elucidated (Vidgren et al., 1999). The loop region between the β1-sheet and αA helix contains a consensus sequence (GAXXG in S-COMT) associated with AdoMet-binding (Schluckebier et al., 1995) and is where the terminal amino and carboxyl groups of AdoMet are bound. The last residue of the β2-strand, Glu90, forms a hydrogen bond with ribose hydroxyls. The His142 has edge-to-face contacts on the opposite side of the adenine ring. The Trp143 closes the adenine ring of AdoMet into the protein with face-to-edge contact. In the Apo form, the side chains of His142 and Trp143 were observed to occupy the adenine ring-bound site and had edge-to-face contact with each other. The side chain of Arg144 moved to the opposite side of Trp143 and made a π–π stacking interaction. The Glu90 made a hydrogen bond with the NH of Trp143 (β4–αD loop) and the amide hydrogen of Ala67 (β1–αA loop) and Asn92 (β2–αB loop) (Fig. 2A and C). The Cα of the Met40 residue moved from the AdoMet site, which was previously reported to be a quaternary complex of S-COMT, to the solvent region of the enzyme by 11.9 Å. The main chain carbonyl oxygen of Met40 made a hydrogen bond with the main chain of Val42 and the side chain had van der Waals contacts with Tyr200. The Oγ of residue Ser119 made a hydrogen bond with the OD1 of Asp150, but Met91 and Gln120 lost hydrogen bond interactions in the absence of an adenine ring. At the N-terminus of the AdoMet-binding pocket, a sulfate ion, from the crystallization buffer interacted with the loop structure constructed from Tyr68 to Ser72. The OD2 atom of Asp141 and the amide hydrogen atoms of Ser72 and Tyr68 made hydrogen bonds with the sulfate ion, and the side chain of the Asp141 residue made a salt bridge with the N^z atom of Lys46. The carbonyl oxygen of Gly66 directly interacted with the NH_2 of AdoMet. However, it was skewed in the Apo enzyme by 31.5°, and an interaction partner could not be detected. A schematic representation of the AdoMet site is shown in Fig. 2D. In Holo form, amino acid residues contained in AdoMet recognition sequences (β1–αA) interacted with AdoMet in the same manner as that of the quaternary structure (Fig. 2B and C). The side chain of Trp143 did not interact with the adenine ring of AdoMet, but the indole ring had van der Waals contact with the side chain of the symmetrically related Glu56. We suppose that Trp143 was trapped in the intermediate state of structural changes from Apo to Holo forms during crystallization.

3.3. Ligand-bound site

Results of previous crystallographic studies indicated that the catalytic site of S-COMT was formed by the Mg^{2+} ion and amino acids important for substrate-binding and catalysis for the methylation reaction. In addition, Lys144 and Glu199 participated in the methylation reaction (Woodard et al., 1980; Vidgren and Ovaska, 1997), and Trp38 and Pro174 were positioned at the surface of the enzyme and sandwiched the planar catechol ring system (Bonifacio et al., 2002; Vidgren et al., 1994; Lerner et al., 2001) to maintain the proper positioning for catalytic reaction. Leu198, Met201, and Trp38 made a hydrophobic wall around the ligand-binding site. Met201 has variable conformations depending on the bound ligand and adjusts the size of the ligand-binding site (Bonifacio et al., 2002). Here, in the absence of AdoMet, a catalytic site of S-COMT could not be formed distinctly. A large Y-shaped cavity newly appeared instead; the aromatic side chains of His142, Tyr68, and Trp38 made a π-electron clustered wall, and Asp169, Asp141, Lys46, and Ser72 made a hydrophilic amino acid cluster. At the center of the cavity, the sulfate ion interacted with the side chain of Asp141. The Cα positions of Asp141, Asp169, and Asn170 in the Apo form were almost identical to those of previously published structure. However, the side chain conformations of these amino acids were quite different. The side chain of Asp141 made a hydrogen bond with the sulfate ion, and the side chain of Asp169 make a hydrogen bond with the N^z atom of Lys46. Asn170 had no interactions with other amino acids, and the Cα of the Glu199 residue moved by 13.7 Å and was exposed to the solvent region (Fig. 3A, top). There were no critical packing interactions from surrounding S-COMT molecules. The side chain of Glu199 had a π–π stacking interaction with the side chain of Tyr200. The Lys144 residue flipped away from the catalytic site and was also exposed to the solvent. Trp38 and Pro174 containing α2–α3 and β5–αE loops adopted an open form compared with the quaternary complex of S-COMT. The Trp38 residue made van der Waals contact with the side chain of Val42 and Cys33. The side chain of Tyr71 made a CH–π interaction with the indole ring of Trp38. The Pro174 residue was exposed to the solvent region, and no interactions were observed. A schematic representation of the ligand-binding site is shown in Fig. 3B. In Holo form, the Mg^{2+} ion coordinated to the oxygen atoms of the side chains of Asp141, Asp169, and Asn170. Only the β5–αE loop moved to almost the same position as that of the quaternary structure (Fig. 3A, bottom). This result indicates that Pro174 defines the orientation of the substrate around the Mg^{2+} ion and allows access to the methyl group from AdoMet when various sizes of ligands bind. Additionally, Leu198 shifted to almost the same position as the quaternary structure during the structural change from Apo to Holo form. Pro174 and Leu198 are known to contribute significantly to the stabilization of the complex (Learmonth et al., 2004). Furthermore, lipophilic Leu198 influences the regioselectivity of *ortho*- and *meta*-nitrated inhibitors (Palma et al., 2006). From our comparisons between Apo, Holo, and complex structures, Pro174 and Leu198 might define the limitations of ligand size and selectivity. The inhibitor-bound structure revealed that the residues contained in β6–β7 interacted with those in α2–α3. The phenolic hydroxyl of Tyr200 made a hydrogen bond with the side chain of Asn41, and the carbonyl oxygen of Glu199 made a hydrogen bond with the side chain of Trp38. The side chain of Tyr200 fit into the cleft made by the residues in α2–α3. On the other hand, the residues in α2–α3 could not interact with β6–β7 in the Holo form. β6–β7 represented a high B-factor and the side chain of Tyr200 had no interaction partner, which was shown in the complex structure; namely, complex formation with AdoMet and Mg^{2+} ion did not induce the formation of a catechol binding site.

3.4. Insights into catalytic mechanisms

The enzymatic kinetics of S-COMT has been extensively studied and the mechanism is sequentially ordered. First, the Apo enzyme binds AdoMet. Second, an Mg^{2+} ion binds to the enzyme–AdoMet complex. Finally, the ligand binds to the Holo enzyme (Lotta et al., 1995). Results of our crystallographic studies suggested the following. To bind AdoMet, the β4–αD loop flipped and the side chains of Trp143 and His142 then made an adenine ring-binding pocket. The N-6 atom of the adenine ring made a hydrogen bond with Ser119 and Gln120. Concomitantly, Glu90, which is a highly conserved residue in the AdoMet dependent methyl transferase family, broke its hydrogen bond with Trp143 and made a new hydrogen bond with the two hydroxyls of the ribose ring. The main chain of Gly66 on the AdoMet-binding loop became skewed, and the carbonyl oxygen made a hydrogen bond with the NH atom of AdoMet to fix it into the proper position. After AdoMet-binding, Asp141, Asp169, Asn170, two-phenolic hydroxyl of catechol, and a water molecule coordinated the Mg^{2+} ion. Lys46 broke its previ-

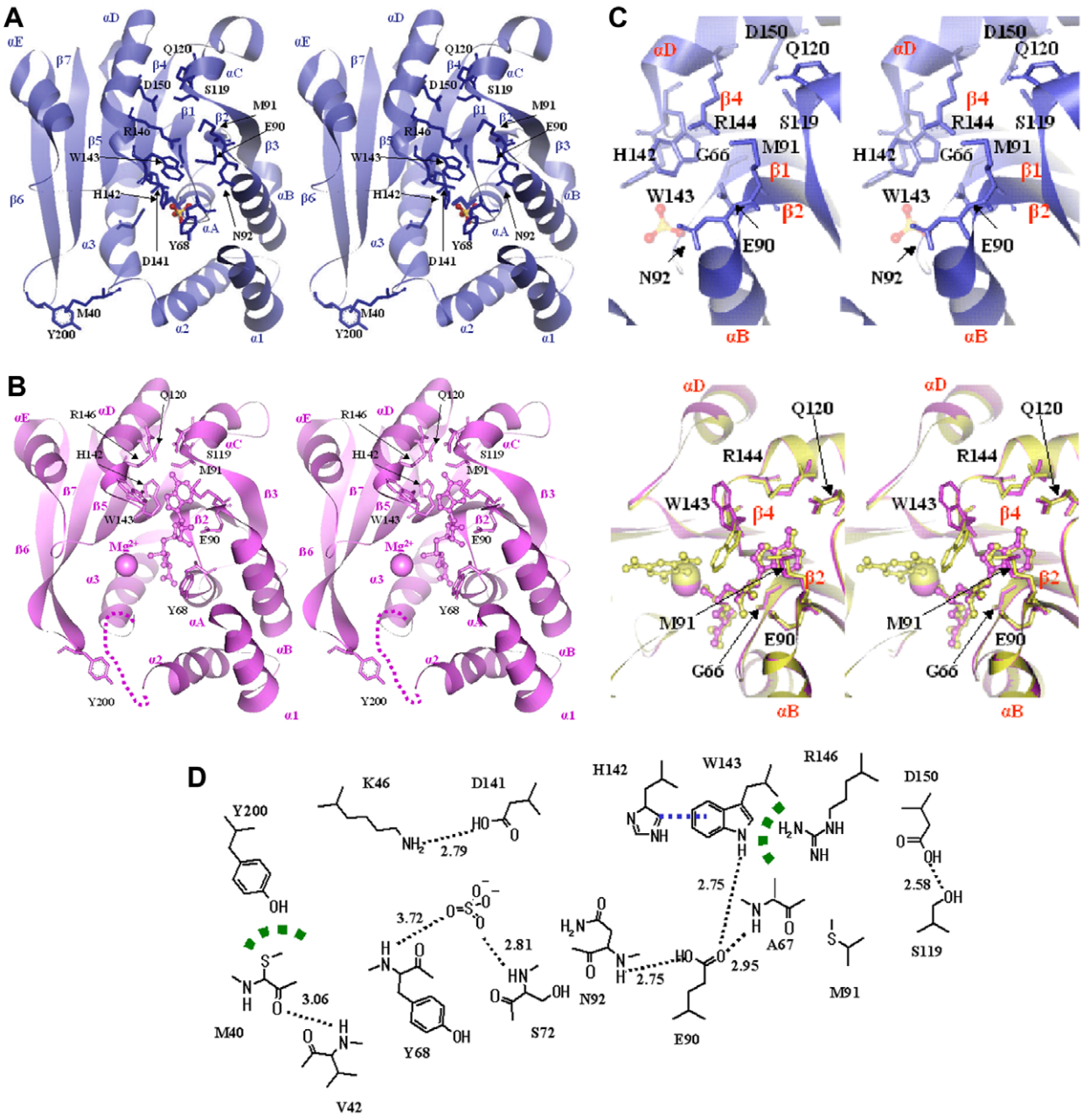

Fig. 2. (A) Ribbon representation of the Apo form of S-COMT. The sulfate ion is depicted as a ball and stick representation. (B) Ribbon representation of the Holo form of S-COMT. The AdoMet is depicted as a stick model. The broken line represents the missing electron density corresponding to residues 36–41. (C, left): Close up view of the AdoMet-biding site of the Apo form. The sulfate ion is depicted as a ball and stick representation. (C, right): Close up view of the AdoMet-binding site of the Holo form and complex structure (PDB code: 1vid). Cyan represents Holo, pale yellow represents 1vid. AdoMet is depicted as a ball and stick representation. (A–C) were produced with WebLab Viewer Lite 5.0 (Accerlys, Japan). (D) Schematic representation of the AdoMet-binding site in the Apo form of S-COMT. Expected hydrogen bond interactions are shown as dotted black lines. Observed distances are given in Å. A CH/π interaction is indicated by a dotted blue line. π–π interactions are indicated as dotted green lines. The figure was produced with ISIS Draw (MDL).

ously formed hydrogen bond with Asp141 and made a new hydrogen bond with Glu199 and Asp169. The N^{z} atom of Lys has been proposed to act as a general base in several proteases and amidases (Paetzel and Dalbey, 1997) and in aspartate aminotransferase (Toney and Kirsch, 1989). By analogy, it seems likely that Lys144 acts as a general base to increase the nucleophilicity of the hydroxyl group of the substrates bound to S-COMT (Zheng and Bruice, 1997). Our structural studies of the Holo enzyme revealed that the side chain of Lys144 and Glu199 was outside of the enzyme as in the Apo form. From this observation, we can assume that Lys144 and Glu199 access the catalytic site only after substrates are bound. In order to access this site, the Cα of Glu199 moved by 5.4 Å and flipped internally. However, the Cα position of Lys144 was the same as the complex structure and seemed to be accessible to the catalytic center without significant conformational change. We thus propose that the side chain of Lys144 moved to the catalytic site first and then the phenolic hydroxyl was deprotonated. Indeed, positively charged Lys144 and *S*-Met group of AdoMet influence the electrostatic effects of catechol ring substitution and the selectivity of various inhibitors (Lautala et al., 2001; Palma et al., 2006). In order to accommodate the ligand into the enzyme, the α2–α3 loop, β5–αE, and β6–β7 loops were found close to the catalytic center. Results of molecular dynamics simulations of S-COMT/3,5-dinitrocatechol complex have indicated that

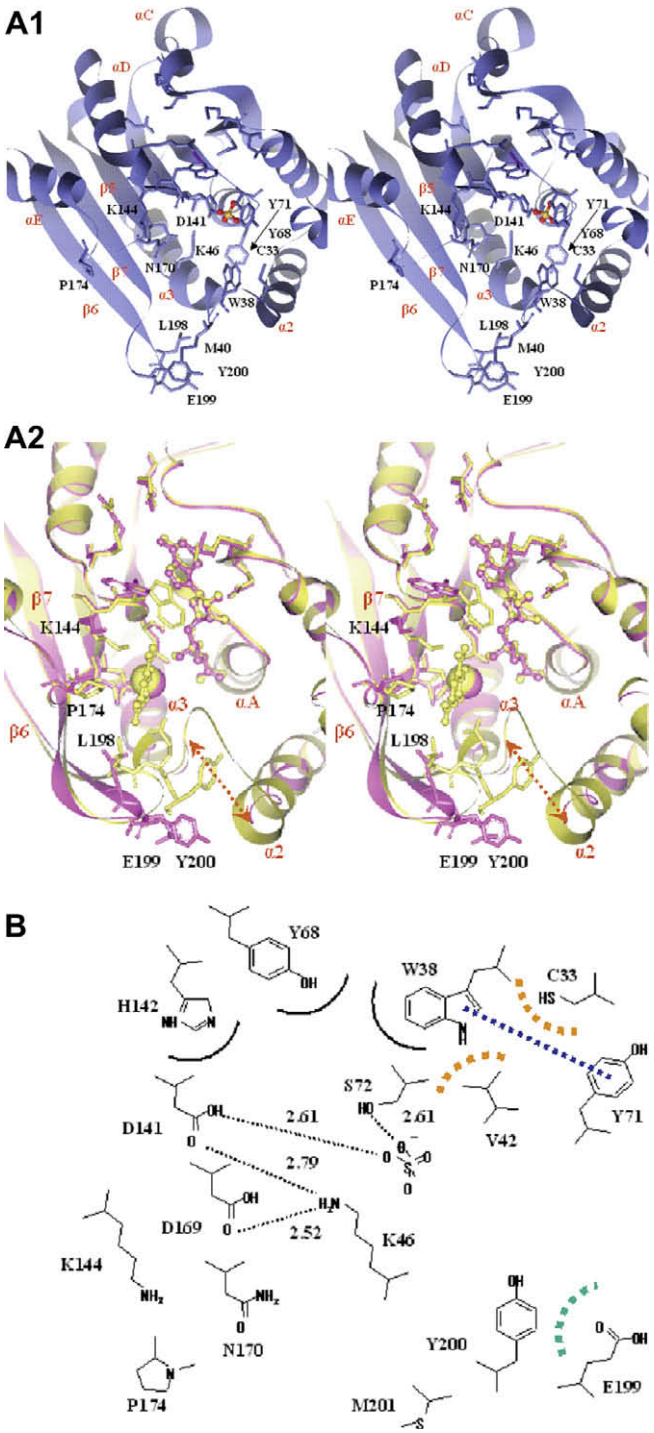

Fig. 3. (A, top): Close up view of the ligand-binding site of the Apo form. The sulfate ion is depicted as a ball and stick representation. (A, bottom): Close up view of ligand-binding site of the Holo form and complex structure (PDB code: 1vid). Cyan represents Holo, pale yellow represents 1vid. AdoMet and 3,5-dinitrocatechol are depicted as ball and stick representations. The CPK represents the Mg^{2+} ion. The broken arrows represent the missing electron density corresponding to residues 36–41. These figures were produced with WebLab Viewer Lite 5.0 (Accerlys, Japan). (B) A schematic representation of the newly created site in the Apo form of S-COMT. Expected hydrogen bond interactions are shown as dotted black lines. Observed distances are given in Å. A CH/π interaction is indicated as a dotted blue line. A π–π interaction is indicated as a dotted green line. van der Waals interactions are represented by dotted orange lines. The figure was produced with ISIS Draw (MDL).

Tyr200, which is contained in the β6–β7 loop, shifts by approximately 1.5 Å towards Trp38, forming a hydrophobic pocket in the vicinity of the 5-position of the catechol ring (Edmond and Thomas, 1998). In the Apo form, the side chain of Trp38 had an edge-to-face interaction with the phenolic ring of Tyr71, but not with that of Tyr200. Additionally, the side chain of Trp38 was not fully visible in electron density; its indole group, which was shielded from the solvent, was disordered. To recognize the substrate in the catalytic cycle, the side chain of Tyr200 moved toward the substrate-bound site by 12.6 Å (Cα distance) and made a hydrophobic accommodation pocket with Trp38. As mentioned in Section 3.3, the α2–α3 loop showed a conformational disorder occurring upon co-factor binding. To promote the catalytic reaction, α2–α3 moved to the catalytic center and need to adopt a close conformation through interaction with β6–β7. Based on analysis of the ground state (containing AdoMet, catechol, and protonated Lys144), the cationic sulfur of AdoMet is presumed to have a significant stabilizing influence with the polar carbonyl of Met40 (Edmond and Thomas, 2000). Taken together, the interaction between β6–β7 and α2–α3 might be essential in the formation of a distinct ligand-binding pocket. Structural studies on the complex with bisubstrate inhibitors have revealed that the appropriate choice of adenine and ribose rings are needed to bind their catechol moiety into the catechol pocket efficiently (Lerner et al., 2001; Masjost et al., 2000; Paulini et al., 2006). This is in agreement with our findings in that there was no AdoMet and ligand-binding site in the Apo form. The AdoMet and Mg^{2+} ion provided a coordination sphere so that catechol could bind properly and a distinct catalytic site was created only after the ligands were bound.

In conclusion, this report describes the crystal structure of S-COMT in two different forms. Our findings reveal that the plasticity of S-COMT upon binding the co-factor and substrate/inhibitor. The conformational change of the ligand-binding domain was much larger than that of AdoMet-binding domain. The structures of Apo and Holo forms thus allow one to understand the mechanistic basis for activation of S-COMT as a potential therapeutic target for treating PD.

4. PDB Accession code

Protein Data Bank: atomic coordinates and structure factors have been deposited with Accession codes 2ZLB and 2ZTH.

Acknowledgments

We are grateful to Dr. Y. Katsuya and the staff of SPring-8 BL32B2 for assistance in X-ray data collection.

References

Bonifacio, M.J., Archer, M., Rodrigues, M.L., Matias, P.M., Learmonth, D.A., Carrondo, M.A., Soares-Da-Silva, P., 2002. Kinetics and crystal structure of catechol-*O*-methyltransferase complex with co-substrate and a novel inhibitor with potential therapeutic application. Mol. Pharmacol. 62, 795–805.

Bunker, A., Mannisto, P.T., St. Pierre, J.-F., Rog, T., Pomorski, P., Stimson, L., Karttunen, M., 2008. Molecular dynamics simulations of the enzyme catechol-*O*-methyltransferase: methodological issues. SAR QSAR Environ. Res. 19, 179–189.

CCP4: Collaborative Computational Project Number 4, 1994. The CCP4 suite: programs for protein crystallography. Acta Crystallogr. D50, 760–763.

Edmond, Y.L., Thomas, C.B., 1998. Importance of correlated motions in forming highly reactive near attack conformations in catechol *O*-methyltransferase. J. Am. Chem. Soc. 120, 12387–12394.

Edmond, Y.L., Thomas, C.B., 2000. Comparison of the dynamics for ground-state and transition-state structures in the active site of catechol-*O*-methyltransferase. J. Am. Chem. Soc. 122, 7165–7171.

Guldberg, H.C., Marsden, C.A., 1975. Catechol-*O*-methyltransferase: Pharmacological aspects and physiological role. Pharmacol. Rev. 27, 135–206.

Kaakkola, S., Gordin, A., Jarvinen, M., Wikberg, T., Schultz, E., Nissinen, E., Pentikäinen, P.J., Rita, H., 1990. Effect of a novel catechol-*O*-methyltransferase inhibitor, nitecapone, on the metabolism of L-dopa in healthy volunteers. Clin. Neuropharmacol. 13, 436–447.

Karhunen, T., Tilgmann, C., Ulmanen, I., Julkunen, I., Panula, P., 1994. Distribution of catechol-*O*-methyltransferase enzyme in rat tissues. J. Histochem. Cytochem. 42, 1079–1090.

Lautala, P., Ulmanen, I., Taskinen, J., 2001. Molecular mechanism controlling the rate and specificity of catechol *O*-methyltransferase by human soluble catechol *O*-methyltransferase. Mol. Pharmacol. 59, 393–402.

Learmonth, D.A., Palma, P.N., Vieira-Coelho, M.A., Soares-Da-Silva, P., 2004. Synthesis, biological evaluation, and molecular modeling studies of a novel, peripherally selective inhibitor of catechol-*O*-methyltransferase. J. Med. Chem. 47, 6207–6217.

Lerner, C., Ruf, A., Gramlich, V., Masjost, B., Zürcher, G., Joakob-Roetne, R., Borroni, E., Diederich, F., 2001. X-ray crystal structure of a bisubstrate inhibitor bound to the enzyme catechol-*O*-methyltransferase: a dramatic effect of inhibitor preorganization on binding affinity. Angew. Chem. Int. Ed. 113, 4164–4166.

Leslie, A.G.W., 1992. Recent changes to the MOSFLM package for processing film and image plate data. In: Joint CCP4 and ESF-EAMCB Newsletter on Protein Crystallography, vol. 26. Daresbury Laboratory, Warrington, United Kingdom.

Lotta, T., Vidgren, J., Tilgmann, C., Ulmanen, I., Melén, K., Julkunen, I., Taskinen, J., 1995. Kinetics of human soluble and membrane-bound catechol-*O*-methyltransferase: a revised mechanism and description of the thermolabile variant of the enzyme. Biochemistry 34, 4202–4210.

Lundstrom, K., Tilgman, C., Peranen, J., Kalkkinen, K., Ulmanen, I., 1992. Expression of enzymatically active rat live and human placental catechol-*O*-methyltransferase in *Escherichia coli*; purification and partial characterization of the enzyme. Biochim. Biophys. Acta 1129, 149–154.

Männistö, P.T., Kaakkola, S., 1989. New selective COMT inhibitors: useful adjuncts for Parkinson's disease? Trends Pharmacol. Sci. 10, 54–56.

Männistö, P.T., Kaakkola, S., 1999. Catechol-*O*-methyltransferase (COMT): biochemistry, molecular biology, pharmacology, and clinical efficacy of the new selective COMT inhibitors. Pharmacol. Rev. 51, 593–628.

Masjost, B., Ballmer, P., Borroni, E., Zurcher, G., Winkler, F.K., Jakob-Roente, R., Diederich, F., 2000. Structure-based design, synthesis, and in vitro evaluation of bisubstrate inhibitors for catechol *O*-methyltransferase (COMT). Chem. Eur. J. 6, 971–982.

McPherson, A., 1990. Current approaches to macromolecular crystallization. Eur. J. Biochem. 189, 1–23.

Navaza, J., 1994. *AMoRe*: an automated package for molecular replacement. Acta Crystallogr. A 50, 157–163.

Paetzel, M., Dalbey, R.E., 1997. Catalytic hydroxyl/amine dyads within serine proteases. Trends Biochem. Sci. 22, 28–31.

Palma, P.N., Rodrigues, M.A., Bonifacio, A.I., Loureiro, A.I., Learmonth, D.A., Carrondo, M.A., Soares-Da-Silva, P., 2006. Comparative study of *ortho*- and *meta*-nitrated inhibitors of catechol-*O*-methyltransferase: interactions with the active site and regioselectivity of *O*-methylation. Mol. Phamacol. 70, 143–153.

Paulini, R., Trindler, C., Lerner, C., Brandli, L., Schweizer, W.B., Jakob-Roente, R., Zurcher, G., Borroni, E., Diedrich, F., 2006. Bisubstrate inhibitors of catechol *O*-methyltransferase (COMT): the crucial role of the ribose structural unit for inhibitor binding affinity. Chem. Med. Chem. 1, 340–357.

Schluckebier, G., O'Gara, M., Saenger, W., Cheng, X., 1995. Universal catalytic domain structure of AdoMet-dependent methyltransferases. J. Mol. Biol. 247, 16–20.

Tilgman, C., Ulmanen, I., 1996. Purification methods of mammalian catechol-*O*-methyltransferases. J. Chromatogr., B: Anal. Technol. Biomed. Life Sci. 684, 147–161.

Toney, M.D., Kirsch, J.F., 1989. Direct Broensted analysis of the restoration of activity to a mutant enzyme by exogenous amines. Science 243, 1485–1488.

Vidgren, J., Ovaska, M., 1997. Structural aspects in the inhibitor design of catechol-*O*-methyltransferase. In: Pandi, Veerapandian (Ed.), Structure-based Drug Design. Marcel Dekker Inc., pp. 343–363.

Vidgren, J., Svenson, L.A., Lijias, A., 1994. Crystal structure of catechol-*O*-methyltransferase. Nature 368, 354–358.

Vidgren, J., Ovaska, M., Tenhunen, J., Tilgman, C., Lotta, T., 1999. Structure and evolution of AdoMet-dependent methyltransferases. In: Cheng, X., Blumenthal, R.M. (Eds.), *S*-Adenosylmethionine-Dependent Methyltransferases: Structures and Functions. World Scientific, River Edge, NJ, pp. 1–38.

Woodard, R.W., Tsai, M.-D., Floss, H.G., Crooks, P.A., Coward, J.K., 1980. Stereochemical course of the transmethylation catalyzed by catechol-*O*-methyltransferase. J. Biol. Chem. 255, 9124–9127.

Zheng, Y.J., Bruice, T.C., 1997. A theoretical examination of the factors controlling the catalytic efficiency of a transmethylation enzyme: catechol-*O*-methyltransferase. J. Am. Chem. Soc., 8137–8145.

Zücher, G., Da Prada, M., 1982. Rapid and sensitive single-step radiochemical assay for catechol-*O*-methyltransferase. J. Neurochem. 38, 191–195.